

Nonlinear Mechanics of Suspension Beams for a Micromachined Gyroscope

W. O. Davis and A. P. Pisano

Berkeley Sensor and Actuator Center
University of California at Berkeley
497 Cory Hall, Berkeley, CA 94720-1774

ABSTRACT

We present a method for the calculation of the coefficients of cubic stiffening for tether-suspended micromachined systems. The analysis is based on a nonlinear rod theory, and enables the prediction of the maximum achievable motion amplitude prior to the onset of nonlinear behavior. The analysis is applied in detail to a microgyroscope. Comparisons with a finite element model and experimental data are used to validate the analysis, and issues pertaining to the optimal design of the gyroscope's suspension are investigated.

Keywords: MEMS, gyroscope, nonlinear, suspension.

1 INTRODUCTION

MEMS suspension beams are usually treated as lumped-parameter linear springs. Formulas for the spring constants using Bernoulli-Euler beam theory are well-known and can be found in [1-3]. In general, however, the spring force is nonlinearly dependent on the displacement. For example, experimental data showing spring-hardening or spring-softening in the frequency responses of MEMS have been reported in [4-7]. However, analytical results for MEMS have been reported only for a few special cases. Micromachined vibrating clamped-clamped beams are modeled in [8]. For the case of suspended masses, an analysis based on nonlinear Bernoulli-Euler beam theory is reported in [9], but this approach accounts only for the effects of nonlinear bending; the effects of axial deformations are not modeled.

In this paper, a method for computing the constants of the nonlinear components of the restoring force (or torque) is presented, and the formulas are specified for the cubic term. The analysis is based on a nonlinear rod theory, described in [9-11], which accounts for axial deformations as well as nonlinear flexure with shear deformations. The theoretical results are compared with finite element simulations and measured data for the micromachined gyroscope shown in Fig. 1. The authors have previously used a linearized version of the rod theory to construct a continuum model of the suspension of a similar micromachined gyroscope [12].

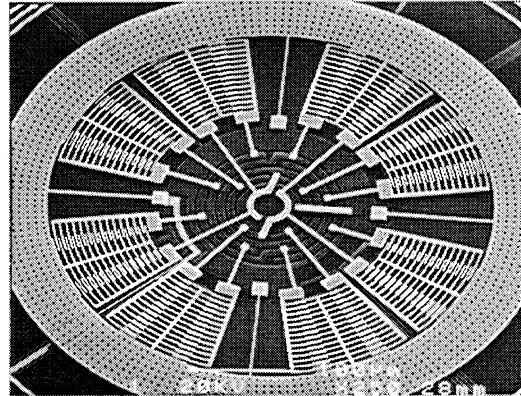


Figure 1: A micromachined gyroscope.

2 ANALYSIS

2.1 Nonlinear Mechanics

We assume that the rotor of the gyroscope is a rigid body, that the four beams are identical with length L , and that the distance from the rotor's centroid to each beam's point of attachment is R . The geometrical parameters and the material properties for polysilicon are listed in Table 1. All displacements are assumed to be in the plane of the device. Let $n_1(x)$ and $n_3(x)$ be the lateral and axial contact force components, respectively, let $M_2(x)$ be the moment, let $u_1(x)$ and $u_3(x)$ be the lateral and axial components of the deflection of the beam axis, respectively, and let $\theta(x)$ be the angle between the cross-section and the undeformed axis. The convected coordinate x locates material points along the beams' axes. We take the following constitutive equations for $n_1(x)$, $n_3(x)$, and $M_2(x)$ [11]:

$$\begin{aligned}
 n_1 &= E A u_1 \left[u_1'^2 + (1 + u_3'^2) - 1 \right] \\
 &\quad + G A k \cos(\theta) \left[u_1' \cos(\theta) - (1 + u_3') \sin(\theta) \right] \\
 &\quad + E I_2 \theta'^2 \sin(\theta) \left[u_1' \sin(\theta) - (1 + u_3') \cos(\theta) \right], \\
 n_3 &= E A (1 + u_3'^2) \left[u_1'^2 + (1 + u_3'^2) - 1 \right] \\
 &\quad - G A k \sin(\theta) \left[u_1' \cos(\theta) - (1 + u_3') \sin(\theta) \right] \\
 &\quad + E I_2 \theta'^2 \cos(\theta) \left[u_1' \sin(\theta) - (1 + u_3') \cos(\theta) \right], \\
 M_2 &= E I_2 \left\{ \left[u_1' \theta' \sin(\theta) - (1 + u_3') \theta' \cos(\theta) \right] \right. \\
 &\quad \left. \left[(1 + u_3') \cos(\theta) + u_1' \sin(\theta) \right] \right\}. \tag{1}
 \end{aligned}$$

For a rotation of the rotor ϕ about its central axis, the restoring torque supplied by the four suspension beams is

$$T_2 = 4 [R n_3(L) \sin(\phi) - R n_1(L) \cos(\phi) - M_2(L)] . \quad (2)$$

Computing the restoring torque requires a solution of the balance laws subject to the appropriate boundary conditions. We assume that the anchors approximate a clamped boundary condition. In summary, the governing equations and boundary conditions for the suspension beams are

$$\begin{aligned} n'_1 &= 0, \quad n'_3 = 0, \quad M'_2 + (1 + u'_3) n_1 - u'_1 n_3 = 0, \\ u_1(0) &= 0, \quad u_3(0) = 0, \quad \theta(0) = 0, \\ u_1(L) &= R \sin(\phi), \quad u_3(L) = R [1 - \cos(\phi)], \quad \theta(L) = \phi. \end{aligned} \quad (3)$$

Because the differential equations are nonlinear, they require a numerical solution. To proceed further analytically, approximations must be employed.

| Parameter | Notation | Value |
|--------------------------------|----------|--------------------|
| Rotor Inner Radius | R | 250 μm |
| Suspension Beam Length | L | 105 μm |
| Suspension Beam Width | w | 1.5 μm |
| Structural Layer Thickness | h | 2.25 μm |
| Cross-Sectional Area | A | h^*w |
| Moment of Area | I_2 | $1/12^* h^*w^3$ |
| Elastic Modulus | E | 160 Gpa |
| Poisson's Ratio | ν | 0.3 |
| Shear Modulus | G | 62 Gpa |
| Shear Coefficient ¹ | k | 1 |

Table 1: Properties of the microgyroscope.

2.2 Approximate Theory

We assume series expansions for the fields:

$$\begin{aligned} n_1(x) &= n_{11}(x)\phi + n_{12}(x)\phi^2 + n_{13}(x)\phi^3 + \dots, \\ n_3(x) &= n_{31}(x)\phi + n_{32}(x)\phi^2 + n_{33}(x)\phi^3 + \dots, \\ M_2(x) &= M_{21}(x)\phi + M_{22}(x)\phi^2 + M_{23}(x)\phi^3 + \dots, \\ u_1(x) &= u_{11}(x)\phi + u_{12}(x)\phi^2 + u_{13}(x)\phi^3 + \dots, \\ u_3(x) &= u_{31}(x)\phi + u_{32}(x)\phi^2 + u_{33}(x)\phi^3 + \dots, \\ \theta(x) &= \theta_1(x)\phi + \theta_2(x)\phi^2 + \theta_3(x)\phi^3 + \dots \end{aligned} \quad (4)$$

The third order approximation to the restoring torque is

$$\begin{aligned} T_2 \approx & 4 [-R n_{11}(L) - M_{21}(L)] \phi \\ & + 4 [-R n_{12}(L) + R n_{31}(L) - M_{22}(L)] \phi^2 \\ & + 4 \left[\frac{1}{2} R n_{11}(L) - R n_{13}(L) + R n_{32}(L) - M_{23}(L) \right] \phi^3. \end{aligned} \quad (5)$$

¹ The shear coefficient, $k = 1$, is due to Rubin [13].

To calculate the approximate torque in Eq.(5), one must solve Eq.(3) at each order in ϕ . The resulting expressions are

$$\begin{aligned} T_2 &\approx -K_1 \phi - K_2 \phi^2 - K_3 \phi^3, \\ K_1 &= \frac{16 E I_2 [G A k (L^2 - 3 L R + 3 R^2) + 3 E I_2]}{G A k L^3 + 12 E I_2 L}, \\ K_2 &= 0, \quad K_3 = \frac{\beta}{1575 E A L^3 (G A k L^2 + 12 E I_2)^4}. \end{aligned} \quad (6)$$

The expression for β , as well as additional details regarding the derivation of Eqs.(6), can be found in [14].

2.3 Physics of Axial Deformations

A comparison of the approximate axial displacement profile $u_{32}(x)$, the exact axial displacement $u_3(x)$ calculated by numerically solving Eqs.(3), and the axial displacement calculated with large-displacement FEA² is shown in Fig. 2. The suspension beams undergo tensile deformations near the anchors and compressive deformations near the rotor. The theoretical results predict less axial deformation at the rotor than does the FEA. The discrepancy may be due to elastic compliance in the rotor, which is neglected in the theoretical analysis.

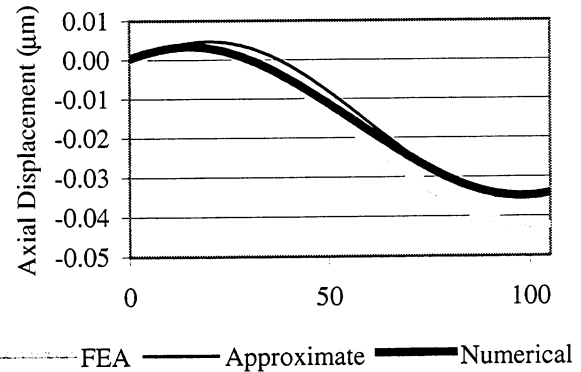


Figure 2: Axial deformation of a suspension beam for a static rotation of the rotor of $\phi = 1^\circ$.

3 COMPARISON WITH EXPERIMENTS

The frequency response of the gyroscope was measured electronically using an off-chip amplifier. The tests were conducted at a pressure of 22 mTorr and with a DC bias voltage of 5 V. For applied AC excitation voltages of 1 mV, 5 mV, and 10 mV, the measured and theoretical amplitude frequency response curves are shown in Fig. 3. The jump frequencies are accurately predicted by the analysis.

² The model was simulated with ANSYS 5.6 using the analysis option NLGEOM.

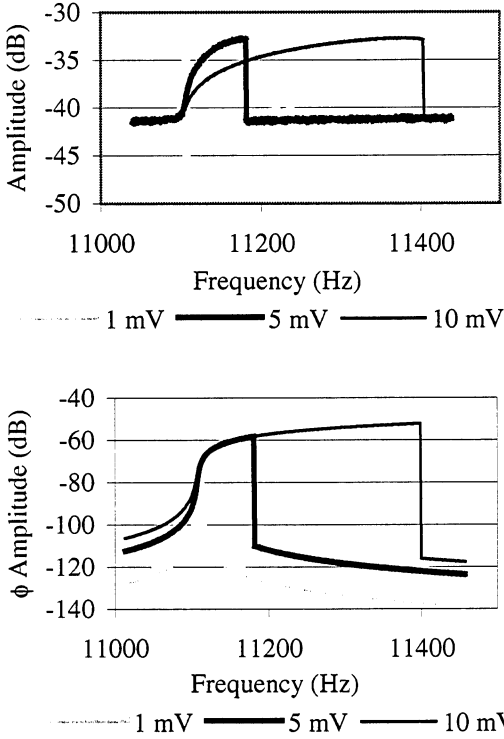


Figure 3: Measured (upper plot) and theoretical (lower plot) frequency response curves showing spring-hardening.

4 OPTIMAL MECHANICAL DESIGN

When the dimensions of the cross-section are small compared to R and L , i.e. $\{w, h\} \ll \{R, L\}$, then shear is negligible, and K_1 and K_3 reduce to the following simplified expressions:

$$\begin{aligned} K_1 &= \frac{4EI_2}{L^3} (L^2 - 3LR + 3R^2), \\ K_3 &= \frac{4EA}{225L^3} (L^2 - 9LR + 9R^2)^2. \end{aligned} \quad (7)$$

We now consider the radius R to be a fixed design parameter and consider suspension designs which minimize the nonlinear behavior. It should be noted that $K_3 = 0$ for $R/L = (0.873, 0.127)$. Physically, these optima arise from the cancellation of spring-stiffening nonlinear flexure and spring-softening effects such as that arising from the axial compression of the beams at their points of attachment with the rotor. A four-beam suspension design in a process with a single structural layer is constrained by the inequality $R/L > 1$. To minimize K_3 , then, the anchors should be set as near to the center of the rotor as possible.

Minimizing K_3 without annihilating it, however, may not minimize the overall nonlinearity, because designs that reduce K_3 also tend to reduce K_1 , resulting in a larger displacement amplitude for a given applied torque.

Therefore, a better strategy is to minimize the ratio of cubic and linear contributions to the restoring torque, which we define as an objective function, J :

$$J = \frac{K_3 |\phi|^3}{K_1 |\phi|} = \frac{K_3}{K_1} |\phi|^2. \quad (8)$$

The amplitude at resonance is

$$|\phi| = \frac{T_{\text{applied}}}{K_1} Q, \quad (9)$$

where T_{applied} is the amplitude of the periodic applied torque, and Q is the quality factor. For a given applied torque and quality factor, and assuming slender beams,

$$\frac{57600 E^2 I_2^3 J}{A R^4 T_{\text{applied}}^2 Q^2} \approx \frac{\frac{L}{R} \left[1 - 9 \frac{R}{L} + 9 \left(\frac{R}{L} \right)^2 \right]^2}{\left\{ \frac{R}{L} \left[1 - 3 \frac{R}{L} + 3 \left(\frac{R}{L} \right)^2 \right] \right\}^3}. \quad (10)$$

The plot of the right-hand side of Eq.(10) as a function of R/L , shown in Fig. 4, indicates that, for designs constrained by the inequality $R/L > 1$, designing the suspension with shorter beams reduces the nonlinear effect. The rate of nonlinearity reduction decreases for beams shorter than $L = 1/2 R$. These further improvements result from decreasing the amplitude of vibration, which in turn tends to reduce the gyroscope's sensitivity. We note that this and other design considerations may outweigh an optimization of the nonlinear stiffness. However, the above analysis provides a means of evaluating the inherent trade-offs.

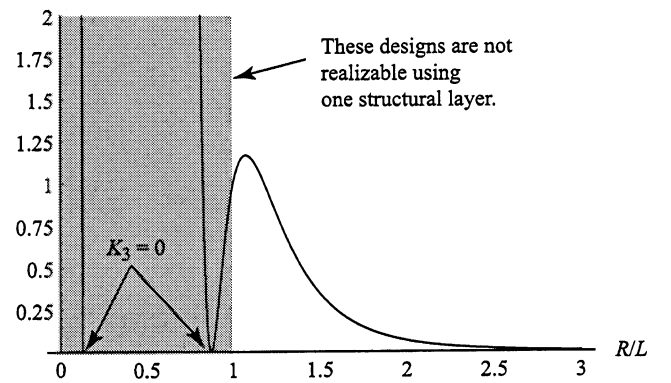


Figure 4: Non-dimensionalized ratio of the cubic and linear contributions to the restoring torque.

5 CONCLUSIONS

We have derived formulas for the cubic stiffening component of the restoring torque supplied by the

suspension beams for a microgyroscope. The theory correctly models the physics of the axial deformations, and gives a good prediction of the frequency response characteristics of the microgyroscope. Formulas are given in the Appendix for two additional suspension designs common in MEMS.

REFERENCES

- [1] Tang, W. C., Nguyen, T. C. H., and Howe, R. T., 1989, "Laterally driven polysilicon resonant microstructures," *Sensors and Actuators*, **20**, 25-32.
- [2] Juneau, T., 1997, "Micromachined dual input axis rate gyroscope," Ph.D. thesis, University of California at Berkeley, Berkeley, CA.
- [3] Fedder, G. K., 1994, "Simulation of microelectromechanical systems," Ph.D. thesis, University of California at Berkeley, Berkeley, CA.
- [4] Pratt, R. I., et al., 1991, "Micromechanical structures for thin film characterization," Proceedings, *Proc. 6th International Conference on Solid-State Sensors and Actuators (Transducers '91)*, San Francisco, CA, 205-208.
- [5] Fujita, T., et al., 2000, "Disk-shaped bulk micromachined gyroscope with vacuum sealing," *Sensors and Actuators A*, **82**, 198-204.
- [6] Yao, J. J., and MacDonald, N. C., 1996, "A micromachined, single-crystal silicon, tunable resonator," *Journal of Micromechanics and Microengineering*, **6**, 257-264.
- [7] Tilmans, H. A. C., and Legtenberg, R., 1994, "Electrostatically driven vacuum-encapsulated polysilicon resonators. Part II. Theory and performance," *Sensors and Actuators A*, **45**, 67-84.
- [8] Judy, M. W., 1994, "Micromechanisms using sidewall beams," Ph.D. thesis, University of California, Berkeley, Berkeley, CA.
- [9] Naghdi, P. M., 1980, "Finite deformation of elastic rods and shells," Proceedings, *Proceedings of the IUTAM Symposium on Finite Elasticity*, Bethlehem, PA, 1982, 47-103.
- [10] Green, A. E., and Laws, N., 1973, "Remarks on the theory of rods," *Journal of Elasticity*, **3**(179-184).
- [11] O'Reilly, O. M., 1998, "On constitutive equations for elastic rods," *International Journal of Solids and Structures*, **35**(11), 1009-1024.
- [12] Davis, W., and Pisano, A. P., 1998, "On the vibrations of a MEMS gyroscope," Proceedings, *Modeling and Simulation of MEMS*, Santa Clara, CA, April 6-9, 1998.
- [13] Rubin, M. B., 1996, "Restrictions on nonlinear constitutive relations for elastic rods," *Journal of Elasticity*, **44**, 9-36.
- [14] <http://bsac.eecs.berkeley.edu/archive/wdavis>

APPENDIX

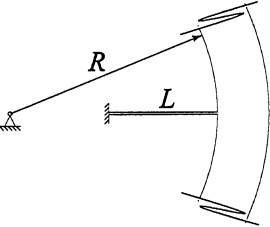
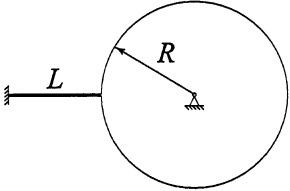
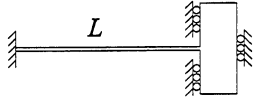
| | | | | |
|-------|-------------------------|---|--|---|
| | |  |  |  |
| K_1 | Shear included | $K_1 = \frac{4EI_2 [Gak(L^2 - 3LR + 3R^2) + 3EI_2]}{GakL^3 + 12EI_2L}$ | $K_1 = \frac{4EI_2 [Gak(L^2 + 3LR + 3R^2) + 3EI_2]}{GakL^3 + 12EI_2L}$ | $K_1 = \frac{12GakEI_2}{GakL^3 + 12EI_2L}$ |
| | $\{w, h\} \ll \{L, R\}$ | $K_1 = \frac{4EI_2}{L^3} (L^2 - 3LR + 3R^2)$ | $K_1 = \frac{4EI_2}{L^3} (L^2 + 3LR + 3R^2)$ | $K_1 = \frac{12EI_2}{L^3}$ |
| K_3 | Shear included | $K_3 = \frac{\beta/4}{1575EAL^3 (GakL^2 + 12EI_2)^4}$ | $K_3 = \frac{\sigma/4}{1575EAL^3 (GakL^2 + 12EI_2)^4}$ | $K_3 = \frac{\eta}{175EAL^3 (GakL^2 + 12EI_2)^4}$ |
| | $\{w, h\} \ll \{L, R\}$ | $K_3 = \frac{4EA}{225L^3} (L^2 - 9LR + 9R^2)^2$ | $K_3 = \frac{4EA}{225L^3} (L^2 + 9LR + 9R^2)^2$ | $K_3 = \frac{252EA}{175L^3}$ |

Table 2: First and third stiffness coefficients for three suspensions commonly used in MEMS. Each coefficient is for one suspension beam. The lengthy expressions for β , σ , and η can be found in [14].